LAWRENCE
LIVERMORE
NATIONAL
LABORATORY

UCRL-JRNL-210479-REV-1

Detection and Tracking of the Back-Reflection of KDP Images in the Presence or Absence of a Phase Mask

A. A. S. Awwal, W. A. McClay, W. S. Ferguson, J. V. Candy, J. T. Salmon, P. J. Wegner

October 20, 2005

Applied Optics

Disclaimer

Detection and Tracking of the Back-Reflection of KDP Images in the presence or absence of a Phase mask

Abdul A. S. Awwal, Wilbert A. McClay, Walter S. Ferguson, James V. Candy, Thad Salmon, and Paul Wegner

University of California, Lawrence Livermore National Laboratory, National Ignition Facility, Livermore, CA. 94551

Abstract

The potassium dihydrogen phosphate (KDP) crystals present in the final optics assembly at the National Ignition Facility (NIF) are used for conversion of infrared laser light beam into ultraviolet. The conversion is highest for a certain incident angle, the alignment of which is determined from the position of the back reflection beam, which exhibits a distinct characteristics shape. When a phase plate device is introduced before the final assembly to increase the uniformity of the beam, the back reflection pattern changes drastically. The algorithm which is best for tracking the special shaped beam is no longer suitable to track the phase modified beam. The work presented here discusses our detection schemes for both the situations. In particular, we demonstrate how the algorithm senses the modified beam using a newly proposed criterion of "correlation peak pedestal area" and execute an alternate algorithm in real time without operator intervention. This new algorithm continuously tracks the beam pattern to guarantee reliable and repeatable

sensing. Results from simulation and real world implementation of the algorithm at the NIF facility are presented.

OCIS codes: 000.5490,70.5010,100.5010,100.5090,120.1880,190.2620

1. Introduction

The National Ignition Facility (NIF), currently under construction at the Lawrence Livermore National Laboratory, is a stadium-sized facility containing a 192-beam, 1.8-megajoule, 500-terawatt, ultraviolet laser system for the study of inertial confinement fusion and the physics of matter at extreme energy densities and pressures [1]. Automatic alignment is one of the most important operations on NIF, which requires high accuracy and fault tolerance. At the heart of this technique is a class of beam position detection algorithms. The algorithms determine the position of the beam along the beam path. A control system uses the output of the algorithm such as the actual and desired beam positions to control mirrors and other optical components to sequentially align the beam from the beginning master oscillator to the final target chamber. The whole autoalignment is thus able to operate with few human operators aided by the intelligent autonomous algorithms. One such algorithm performing task specific detection is elaborated here. Before reaching the target chamber the beam must pass through a pair of potassium dihydrogen phosphate (KDP) crystals. The beam alignment is performed using the reflection from the back surface of one crystal. The determination of the position of the KDP back-reflection beam has been a long-standing challenge for the automatic alignment of the KDP

crystals at NIF, because of the constant fluctuation of the beam position estimated by a simple centroiding algorithm and the variability of the crystal reflected wavefront.

The KDP crystals act as a frequency converter to harmonically convert the infrared laser light to ultraviolet. They produce maximum gain for a certain tilt angle. This angular tilt must be determined from the position of the back-reflection of the frequency conversion crystals. The KDP crystal angle must be adjusted within ±20 μrad over a field of view of ±200 μrad. Due to gravity and other effects, the KDP crystals exhibit a sag, which introduces a phase aberration into the beam. As a result, the beam reflected from the second KDP surface suffers from phase distortion, and produces a diamond shaped beam pattern. The challenge is to find a stable measurement of the beam position, which should remain stable if no mechanical movement of the crystal occurs.

A *weighted centroid* was used to determine the position of the back-reflection. However, due to local intensity variation, termed "boiling noise", the weighted centroid position varies significantly from frame to frame. To overcome this problem, a *binary centroid* was used. It was expected that binarization would hide the variation of intensity. However, since binarization is a function of the threshold value used, as the image intensity varies the centroid position varies by 8 or more pixels in any one direction. Thus an alternate algorithm such as a matched filter is sought.

One of the characteristics of the KDP back-reflection image is the presence of well-defined, relatively stable fringe patterns within the beam as shown in Fig. 1(a). We show that these fringe patterns facilitate a stable beam position detection method based on composite [2] *amplitude modulated phase only matched filter* (AMPOF) [3]. When however, a phase plate is introduced into the beam line, the beam loses its structured shape as shown in Fig. 1(b) and the

AMPOF method fails to the detect the beam. We show how we use a characteristic measure of the correlation output to automate the switching of the algorithm.

The KDP alignment optical hardware is depicted in Figure 2. An alignment beam emanating from a fiber at the focus of the final spatial filter is used to determine the angle of the KDP crystals (as shown in the expanded onset of the dotted circular region). The alignment beam reflects off of a crystal surface and returns to the (transport spatial filter) TSF focus plane where a second fiber source provides a reference at an offset corresponding to perfect alignment. Light from both the reference and the reflected beams is collected at the output sensor package (OSP) by a beam splitter cube and a relay optics system. A centroiding and the KDP algorithm described in this paper are used to calculate the reference and KDP image positions. The difference which serves as the error signal is used to adjust the crystal angle. In case there is a phase plate inserted into the beam, it is placed in front of the vacuum window away from the KDP.

2. Algorithm

VanderLugt was the first to introduce the *classical matched filter* (CMF) for optical pattern recognition [4]. In this method, the complex amplitude and phase of the reference pattern is stored as a hologram. The *phase only filter* (POF) is a variation of the CMF, which uses only the phase of the reference pattern to perform correlation detection [5]. The AMPOF was designed to further enhance the performance of the POF [3]. The mathematical foundation of the AMPOF filter is derived as shown in the following equations. Let the Fourier transform of the object function $f(x,y)$ be denoted by:

$$F(U_x, U_y) = \left|F(U_x, U_y)\right| \exp(j\Phi(U_x, U_y)) \tag{1}$$

Then a CMF corresponding to this function *f*(x,y) is expected to produce its autocorrelation. From the Fourier transform theory of correlation, the CMF is given by the complex conjugate of the input Fourier spectrum as denoted by Equation 2.

$$H_{CMF}(U_x, U_y) = F^*(U_x, U_y) = \left|F(U_x, U_y)\right| \exp(-j\Phi(U_x, U_y)) \tag{2}$$

The inverse Fourier transformation of the product of $F(U_x, Uy)$ and $H_{CMF}(U_x, Uy)$ results in the convolution of *f*(x, y) and *f*(-x, -y), which is the equivalent of the autocorrelation of *f*(x, y). Moreover, when $|F(U_x, Uy)|$ is set to unity, H_{CMF} becomes a *phase only filter* (POF) as shown in Equation 3.

$$H_{POF}(U_x, U_y) = \exp(-j\Phi(U_x, U_y)) \tag{3}$$

Since the convolution operator in the spatial domain is equivalent to the product operator in the frequency domain, one can think of the POF as an edge enhancer by way of division by $| F(U_x, Uy) |$. To get an even sharper peak, it is useful to divide the H_{POF} by a magnitude function, which will lead to an impulse type of correlation. An AMPOF attempts to achieve exactly this. The generalized AMPOF filter is expressed as [6]:

$$H_{AMPOF}(U_x, U_y) = \frac{aF^*(U_x, U_y)}{\left[\ b + c\left|F(U_x, U_y)\right| + d\left|F(U_x, U_y)\right|^2\ \right]^m} \tag{4}$$

When, a = b = m = 1, c = d = 0, this results in the classical matched filter; when b = d = 0, a = c, m = 1 it results in a phase only filter expressed by Equation 3. When b is a small constant for

nonzero values of a, c, and d it is an AMPOF. The AMPOF described in [3] has a = constant, d = constant, c = 0, m = 1 and b = ε (a small constant number). It was found, after some experimentation, that when b = ε, d = 0 and c = a = 1, better stability of position detection results in the current KDP beam. More detailed optimization of these parameters is possible [7,8]. The AMPOF correlation of the input image and the target is simply:

$$C_{AMPOF}(\Delta_x, \Delta_y) = F^{-1}\{F(U_x, U_y) H_{AMPOF}(U_x, U_y)\} \tag{5}$$

As can be seen from Figure 1(b), in the presence of phase plate the beam looses its spatial characteristics, which is necessary for its detection. The change is caused by the presence of a beam shaping device in the focal plane of the final focus lens. The device in the form of a phase plate is used to increase the beam uniformity when averaged over a small area. From the physics-based simulation of the KDP back-reflection, it is known that the position of the beam should be its weighted centroid if the camera has an infinite dynamic range [9]. In other words, in the absence of the phase distortion caused by the KDP crystal, the beam will converge to the weighted centroid of the back-reflection caused by the KDP crystals. Thus, if we know the original position of the KDP template, then by knowing the displacement from the current position we can calculate its new absolute position. By knowing the position of the cross-correlation peak, we can determine the relative displacement of the KDP beam with respect to its current position by subtracting the position of the autocorrelation peak for the template from the cross-correlation position. Let the position of the original reference KDP beam be (x_c, y_c). Then the position of the KDP pattern after matched filtering is given by:

$$x_{pos} = x_{cross} - x_{auto} + x_c \tag{6}$$

$$y_{pos} = y_{cross} - y_{auto} + y_c \tag{7}$$

where (x_{pos}, y_{pos}) is the position of the KDP, (x_{auto}, y_{auto}) is the position of the template autocorrelation peaks, and (x_{cross}, y_{cross}) is the position of the cross-correlation peak. The position of the cross-correlation peak was determined using a curve fit to the correlation peak. The center of the template, (x_c, y_c), is determined off-line by careful filtering and calculating its weighted centroid. The position of the autocorrelation peak is also determined off-line. Both of these parameters are constants for the algorithm. They will only change if the templates are modified. A second order curve fit to the correlation peak results in the following expression for the correlation peak positions:

$$X_{cross} = \frac{0.5f_0(x_1 + x_2) + 0.5f_2(x_0 + x_1) - 0.5f_1(x_0 + x_2)}{f_0 - 2f_1 + f_2} \tag{8}$$

where the (x_i, f_i) pair represents the x position versus the intensity pairs. When the pair is replaced by the (y_i, f_i) pairs, it results in the corresponding y-locations.

$$Y_{cross} = \frac{0.5f_0(y_1 + y_2) + 0.5f_2(y_0 + y_1) - 0.5f_1(y_0 + y_2)}{f_0 - 2f_1 + f_2} \tag{9}$$

The pair (x_{cross}, y_{cross}) obtained from Eqs. (8) and (9) is the position of the correlation peak. A block diagram of the overall algorithm is shown in Figure 3.

3. Experimental results

In this section, we describe a series of experiments demonstrating the development of the AMPOF-based position detection scheme. The first experiment was performed using the classical matched filter over a set of 5 consecutive recorded frames without any mechanical movement. The matched filter expressed by Eq. 2, was constructed from the image in the first frame. The correlation peak was detected by a Gaussian fit to the correlation peak. These results are then compared to the existing binary centroid-based algorithm. The centroid position obtained from the binary centroid algorithms and the correlation peak obtained using matched filtering for comparison is shown in Fig. 4. For the centroid-based case, the image shows wide variations of the position data, while the CMF case demonstrates a more stable measurement. The radial standard deviation is estimated for both cases. The radial standard deviation for CMF based detection is 0.99 pixels. This result was a significant improvement over the previous binary centroid-based beam locator, which yielded a radial standard deviation of 9.1 pixels.

One of the problems of peak detection using Gaussian fit algorithm is that it is computationally slow, consuming close to 3 seconds to execute. A second problem is that there is a possibility for some cross-correlations to fail the Gaussian fit. Since the software must work in a real time system, such failure will crash the automated alignment process and valuable experimental time in the NIF facility will be lost. For real-time operation a faster method is preferred. The polynomial curve fit expressed by Eqs. (8) and (9) could be executed in 0.02 seconds, which is approximately 240 times faster than a Gaussian curve fit. Surprisingly, the radial standard deviation improves to 0.60 pixels. Note that the first frame was used as the template for the consecutive frame images. Next, a composite filter was constructed from a

weighted addition of three images. This filter further improved the radial standard deviation to 0.51 pixels.

Next we construct AMPOF using Eq. (4). Since an AMPOF matches the fringe features of the image more than the intensity level, it results in a sharper correlation peak, consequently is expected to yield lower radial standard deviation than CMF. A CMF correlation peak usually has a broad peak, but the correlation peak is smoother. The AMPOF produced more clustered position data compared to the composite CMF. The AMPOF was further optimized by developing a composite AMPOF filter [2,3] which can incorporate some of the frame to frame image variability. The composite AMPOF produced a radial standard deviation of only 0.27 pixels. Although these results are obtained above from a small sample of real world data, Monte Carlo simulation results on a larger sample set shown in the next section demonstrates even better performance than this.

The higher variance of CMF originating from perhaps a wider correlation peak can be explained by analyzing the correlation operation in the Fourier domain. For CMF, the correlation operation (product of Eq. 1 and 2) requires a squaring of the image magnitude and cancellation of the phase. Therefore, the correlation is the average value of the squared magnitude. The squaring introduces higher frequencies, thus transferring energy away from the zero frequency. While this results in a smoother (opposite of a sharp peak) correlation peak, it shows high variability. Additionally, the higher variability is due to its response to the intensity fluctuations inside the specific beam shape. The AMPOF is less immune to the fluctuations since it can ignore the local fluctuation only responding to the fringes of the spatial pattern. Figure 5 illustrates the AMPOF and CMF correlation peaks from these experiments. The sharper

correlation peak reduces the uncertainty number from 0.9 pixels for CMF to 0.27 pixels generated by the AMPOF.

Since the KDP back-reflection images vary with time, the templates should be designed from a series of images, so that the variability is accommodated in the template. The template design utilized the historic database of KDP images from NIF database saved over a six month period of time. The filters were designed by averaging the real KDP images that remained within a two-sigma bound [10], as shown in Fig. 6, after they were registered with respect to each-other.

4. Reliability using Monte Carlo simulation

It should be emphasized that the NIF alignment algorithms must operate with high degree of reliability. In case, there is a high noise in the optical imaging system, this must be accounted for by reporting a high uncertainty about the results. This will allow the control room operators and optical engineers to inspect the system for any flaw or problems in the optical system. Thus one of the requirements of the NIF auto-alignment is to estimate the uncertainty associated with each beam position based on the noise in the image. We describe a method of calculating this uncertainty of this algorithm using Monte Carlo simulation. In the simulation different instances of the real beam image is created with various degrees of signal and noise levels. Thereafter, the algorithm is used to determine the position of this noisy set. The variability of the measured position over a set of images yields an indication about the uncertainty of the position measurement for that set of signal and noise levels.

An image of the real KDP back-reflection is recorded by manually segmenting its bright region. The amplitude of this image is scaled to 200, 100, and 50 to create examples of bright and dim images. White Gaussian noise is added to these image sets with an rms count of 10, 20,

and 50. We create a set of 100 images for each amplitude and rms noise. Figs. 7(a) and 7(b) show examples of noise rms 20 and 50 respectively. The diffraction noise was generated by calculating a sinusoid of an amplitude such as say 20 (for example) and a period λ determined by the nominal size of the object. One λ indicates that the size of the object is equal to the period of the diffraction, a λ/2 indicates that the size of object is equal to half of the period, 2λ indicates the size of the object is two times the period. The noise has both negative and positive values, however, after adding with the image the combined image is truncated at both ends to set the minimum value to the noise floor (which is 20 in our case) and maximum value (which is 255) of saturation limit. Figures 7(c) and 7(d) show example of λ/2 and λ diffraction noise respectively.

Then the algorithm is used to evaluate these images for each signal and noise level and the standard deviation (one-sigma) of the position data is calculated from the scatter plot. The three-sigma is taken as a measure of uncertainty. (It should be cautioned, however, this three-sigma does not guarantee a 99.875% probability of being correct. To calculate uncertainty using a probability approach one needs to fit the distribution and then to evaluate the range within which the measurement should lie 99.875% of time [11].)

The AMPOF based algorithm was evaluated using 900 simulated noisy images as described above. Its performance was compared to that of the binary centroid based algorithm previously operating at the NIF facility. The three-sigma uncertainty curves of these two runs are shown in Figures 8(a) and (b). The centroid based algorithm produces an uncertainty of 17 pixels, with maximum image amplitude 100 and noise rms of 50; the new algorithm produces uncertainty below 0.5 pixels for the same imaging condition as shown in the Figures 8(a) and (b). For these tests, the template was chosen from the undistorted image. From the curve for the

standard case of amplitude 200 and noise count of 20, the three-sigma noise is less than 0.1 pixels. It should be noted that we used a single image to derive our template image and it does not incorporate any variations due to boiling noise. It is possible to use multiple images to incorporate image variability and improve the three-sigma range to an even lower value.

One problem with a real KDP image is that the absolute position is not really known. In order to evaluate the algorithm performance in terms of absolute location versus measured location, another set of 900 images was created from the original shown in Figure 9(a). Note that this image is artificially created, where the center location is either known or can be measured very accurately. Both Gaussian noise and diffraction noise were added to this image. Examples of diffraction pattern added images are shown in Figures 9(b-d).

The AMPOF filter was designed from the original image as shown in Figure 9(a). Interestingly, the interference noise images shown in Figures 9(b–d) illustrate that in some cases 50% of the image is missing. The correlation output for the image in Fig. 9(d) is shown in Fig. 10. Although 50% is missing from the image, it still displays very distinct peak. It should be noted here that a classical matched filter or binary centroiding will be heavily biased towards the illuminated region whereby they will settle to a position of maximum overlap. The AMPOF, on the other hand, matches the edges and thus the result is close to the true location of the object. The uncertainty results with these simulated KDP images are presented in Figures 11 and 12. From Figure 11(a) the amplitude 200 and 100 images with less than or equal to 20 count rms noise show an uncertainty less than the tolerance limit of 0.5 pixels. The results from images corrupted by interference type noise are shown in Figures 11(b) and 12.

Since in this experiment the true centroid position is known with a high degree of accuracy (no noise image), this position was used to calculate the difference between the average

of position readings for each set and the true position. They were found to be bounded by the theoretical maximum of $3\sigma/\sqrt{n}$, where σ is the standard deviation of each set [12]. Even for the worst case where the signal amplitude was low and noise amplitude high, the actual deviation was found to be close to 0.1 as shown in Figure 13(a). The result can also be visualized in the accompanying scatter plot of a specific set in Figure 13(b).

One application of the uncertainty curves is to approximate the uncertainty from the real image. Estimating the noise rms and signal level from the image and then using the curves in Figure 12(a) as a lookup table, one can estimate the uncertainty from the real NIF images while in operation. This allows us to ascertain that the error allowed for the alignment loop is within the error tolerance assigned in the total NIF error budget.

5. Task Specific algorithm switching

All NIF automatic alignment algorithms have three building blocks. A preprocessing stage, an algorithm stage and a post processing stage. The preprocessing usually eliminates simple cases of all dark, dim, or all white images. However, if these images are not rejected by the preprocessing stage then the post-processing will attempt to eliminate those cases. The preprocessing was further enhanced into a process called off-normal image processing. The purpose is to detect abnormal images caused by a mechanical failure of any opto-mechanical components or images from a wrong beam fiducial etc. This is designed to eliminate accidental alignment to wrong beam. In case, such an event is caught, a high uncertainty is flagged. The automatic beam control system is programmed to stop the automated process and enter into a manual controlled mode. The operator must then examine the image and make a decision to reactivate the automated process if appropriate.

It is possible to derive post-processing based on different criteria such as correlation amplitude, normalized correlation peak, average energy correlation peak, average amplitude correlation peak, pedestal area of the correlation peak (under half power points). We experimented with all of these possible parameters. The difficulty in normalizing images with saturated pixels prohibits us from using correlation peak magnitude. The most promising was based on determining the pedestal under half power point.

The effectiveness of the pedestal approach can be explained with a simple experiment of correlating two objects, a circle and a square as shown in Fig. 14. The diameter of the circle is equal to the side of the square. First, a CMF is formulated with the circle object and matched against both the circle and the square. The normalized autocorrelation provides us with a discrimination of 23% while the pedestal measurement provides discrimination of 46%-289% as shown as shown in Table I (exp. 1). Note also that as expected with a circle filter (which completely overlaps with the square), the absolute correlation peak is exactly the same for both auto- and cross-correlation. On the other hand, if we use the square object as the filter (Exp. 2, Table I), normalized autocorrelation provides a 0% discrimination while the pedestal approach yields 18% - 264%! The absolute peak in this case, however, provides some discrimination. Next we formulate the AMPOF filters (Exp3. and Exp. 4). A dramatic improvement of the discrimination ratios in the pedestal measurement is observed compared to the CMF, which ranges from several thousands to hundreds of thousands! Additionally, in the AMPOF the discrimination ratio of the peak or normalized peak is improved to over 75%. Note that all discrimination ratios are calculated by normalizing the difference between auto and cross-parameters by the auto parameters as in abs(auto-cross)/auto, where auto represents the autocorrelation parameters (pedestal, peak etc.) and cross represents the cross correlation

parameters. Also to be noted that pedestal at 0.5 (or 0.9) counts all the pixels that exceed 50% (or 90%) of the peak value in the correlation plane. The normalized peaks are multiplied by 10^5 to make all normalized quantities in the same scale.

Since we are using an AMPOF filter it generally produces a very sharp correlation peak, when there is a match. When the image starts to change relative to the template such multiple targets, and a background or white image or contains high noise counts, the number of peaks (which are mostly false) or the width of the peak increases, as a result the pedestal count increases. In order to find a suitable threshold, images derived from the template image with added noise as well as images from different beam line (derived from different KDP crystals) were subjected to the AMPOF and corresponding pedestal area measured. Images derived from the template are called "in-class" and those from other beam lines are called "out-of-class". The pedestal areas for both of these classes are plotted in Fig. 15. Examining Fig. 15 shows that for the inclass objects the pedestal of the auto-correlation peak is very low, signifying a very narrow peak. The highest of the pedestal areas occur with autocorrelations with high diffraction noise. However, for the images that are significantly different from the template, the pedestal is high. The noisy images produce a correlation with a wider peak or many false peaks, which is less than the absolute maximum, but greater than the noise-free case. Analyzing Fig. 15, a post-processor could be designed to reject a correlation peak with a pedestal above 160. This ensures that it will accept all similar class images but reject all of the out-of-class images. But noticing that the real images are not as noisy, we lowered the threshold to 100 so that most of the noisy images were rejected. This ensures that when the beam pattern starts to change the correlation peak width will also change and be detected. This allows us to update the templates to accommodate the new reflection pattern.

When a phase plate is introduced the pedestal becomes more than several hundred reaching 800 or above values. Thus it is simple to detect this condition and switch to a different algorithm. The alternate algorithm applies a dilation operator multiple times to grow a binary mask which fits the region of the illuminated areas. Then a weighted centroid is performed on that region. By eliminating noisy pixels from outside the region of interest using the dilated mask, a stable measurement is achieved. A block diagram of the algorithm switching mechanism is illustrated in Fig. 16.

6. Conclusions

This work illustrates the use of AMPOF for detecting KDP back reflection. Unlike the correlation peak, it introduces a new correlation criterion known as pedestal area, which can be used as a measure of dissimilar object and facilitates automated switching of algorithm. According to our knowledge, this is the first time this criterion has been used. This criterion can also be used to indicate a change in the beam pattern and consequent need for updating the template.

Other enhancements to the proposed detection algorithm is possible [13,14]. To make the algorithm more accurate with a constantly updated template, it is possible to switch to a tracking algorithm [15,16] where it uses the current image as the template. It can use the stored template to find the position of the new image template. Then this is used in the subsequent iterations to find the positions of consecutive images. In the design of this particular AMPOF we had four different variables to optimize. We used the radial standard deviation as the function to be optimized. Other objective functions to optimize include the correlation peak, or variation in the correlation peaks [7].

Acknowledgement

The authors acknowledge discussions with Dr. Erlan Bliss and Mr. Scott Burkhart about the KDP alignment requirements and Mr. Paul Van Arsdall for useful feedback about the paper. The authors thank the reviewers for their constructive suggestions. This work was performed under the auspices of the U.S. Department of Energy by the University of California, Lawrence Livermore National Laboratory under contract No. W-7405-Eng-48.

References

1. E. I. Moses and C. Wuest, "The National Ignition Facility: Status and Plans for Laser Fusion and High-Energy-Density Experimental Studies", *Fusion Science and Technology*, Vol. 43, pp. 420-427, May 2003.
2. M. Rahman, A. A. S. Awwal, and K. Gudmundsson, "Composite Filters for Search Time Reduction for 3D Model Based Object Recognition," *Photonic Devices and Algorithms for Computing* V, K.M. Iftekharuddin and A. A. S. Awwal, Editors, Proc. of SPIE, Vol. 4201, 2003.
3. A. A. S. Awwal, M. A. Karim, and S. R. Jahan, "Improved Correlation Discrimination Using an Amplitude-Modulated Phase-Only Filter," *Applied Optics*, Vol. 29, pp. 233-236, 1990.
4. A. VanderLugt, "Signal Detection by Complex Spatial Filtering", IEEE Trans. Inf. Theory IT-10, 139-145 (1964).
5. J. L. Horner and J. Leger, "Pattern Recognition With Binary Phase-Only Filters", Appl. Opt. 24, 609-611 (1985).
6. M. A. Karim and A. A. S. Awwal, "Optical Computing: An Introduction", John Wiley, New York, NY, 1992.
7. K. M. Iftekharuddin, M. A. Karim, and A. A. S. Awwal, "Optimization of Amplitude Modulated Inverse Filter", *Mathematical and Computer Modeling*, Vol. 24, pp. 103-112, 1996.

8. K. M. Iftekharuddin, M. A. Karim, P. W. Eloe, and A. A. S. Awwal, "Discretized Amplitude-Modulated Phase-Only filter", *Optics and Laser Technology*, Vol. 28, pp. 93-100, 1996.
9. Personal communications with Paul Wegner at NIF.
10. James V. Beck and Kenneth J. Arnold, Parameter Estimation in Engineering and Science, John Wiley & Sons, New York, 1977.
11. Mike Axelrod, "Modeling image noise that is both non-Gaussian and non-stationary", presented in Photonic Devices and Algorithms for Computing VI, conference Denver, SPIE 5556, August, 2004.
12. J. P. Holman (in collaboration with W. J. Gajda), *Experimental Methods for Engineers*, Chapter 3–11, McGraw-Hill Book Co., 3rd edition, 1978.
13. A. A. S. Awwal and H. E Michel, "Enhancing the Discrimination Capability of Phase Only Filter", *Asian Journal of Physics*, Vol. 8, pp. 381-384, 1999.
14. F. Ahmed, A. A. S. Awwal and M. A. Karim, "Improved Recognition Performance With Synthetic Correlator," *Microwave and Optical Technology Letter*, Vol. 14, pp. 274-278, 1997.
15. Karl S. Gudmundsson, and A. A. S. Awwal, "Sub-Imaging Technique to Improve POF Search Capability", *Applied Optics*, Vol. 42, pp. 4709-4717, 2003.
16. A. A. S. Awwal, W. Mcclay, W. Ferguson, J. Candy, T. Salmon and P. Wegner, "Composite amplitude modulated phase-only filter based detection and tracking of the back-reflection of KDP images," in *Photonic Devices and Algorithms for Computing VI*, edited by K. Iftekharuddin and A. A. S. Awwal,, Proc. of SPIE 5556 (SPIE Bellingham, WA, 2004), pp. 180-190.

List of Tables

Table I. Pedestal experiment comprising a circle and a square object.

Exp. 1: Filter = circle, input object square and circle, CMF			
Features	Auto	Cross	Discrimination ratio
Pedestal at 0.5	9263	13556	46%
Pedestal at 0.9	349	1360	289%
Normalized peak	7.03	5.37	23%
Absolute peak	3011	3011	0%
Exp. 2: Filter = square, input object square and circle, CMF			
Features	Auto	Cross	Discrimination ratio
Pedestal at 0.5	11415	13556	18%
Pedestal at 0.9	373	1360	264%
Normalized peak	5.37	5.37	0%
Absolute peak	3943	3011	23%
Exp. 3: Filter = circle, input object square and circle, AMPOF			
Features	Auto	Cross	Discrimination ratio
Pedestal at 0.5	9	2068	22800%
Pedestal at 0.9	1	24	2300%
Normalized peak	61.23	8.52	86%
Absolute peak	3335	706.86	79%
Exp. 4: Filter = square, input object square and circle, AMPOF			
Features	Auto	Cross	Discrimination ratio
Pedestal at 0.5	57	4400	7600%
Pedestal at 0.9	1	286	28500%
Normalized peak	30.45	6.37	79%
Absolute peak	1932	458	76%

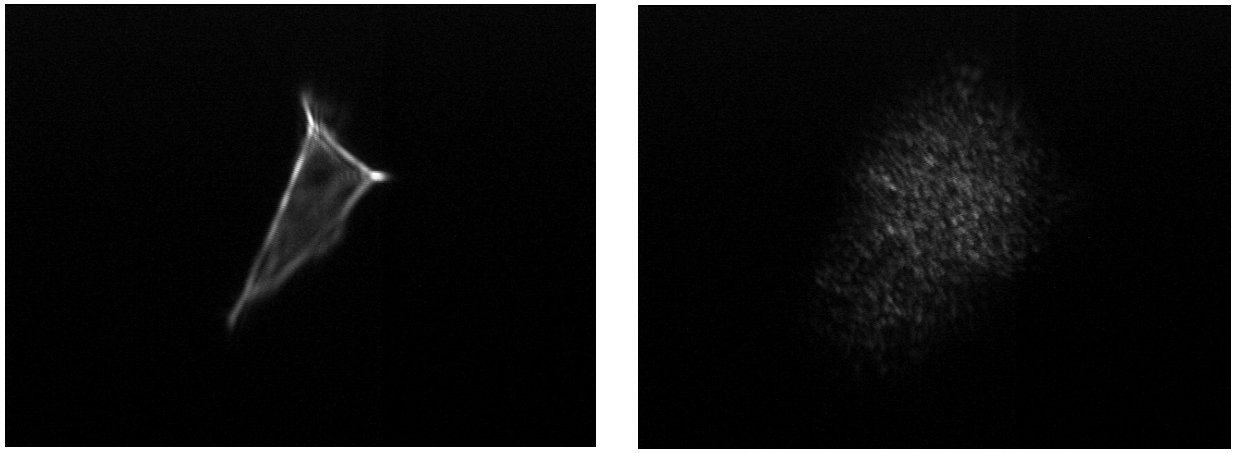

(a) (b)

Figure 1. Example of real KDP back-reflection pattern (a) left image is without a phase plate (b) right image in the presence of a phase plate

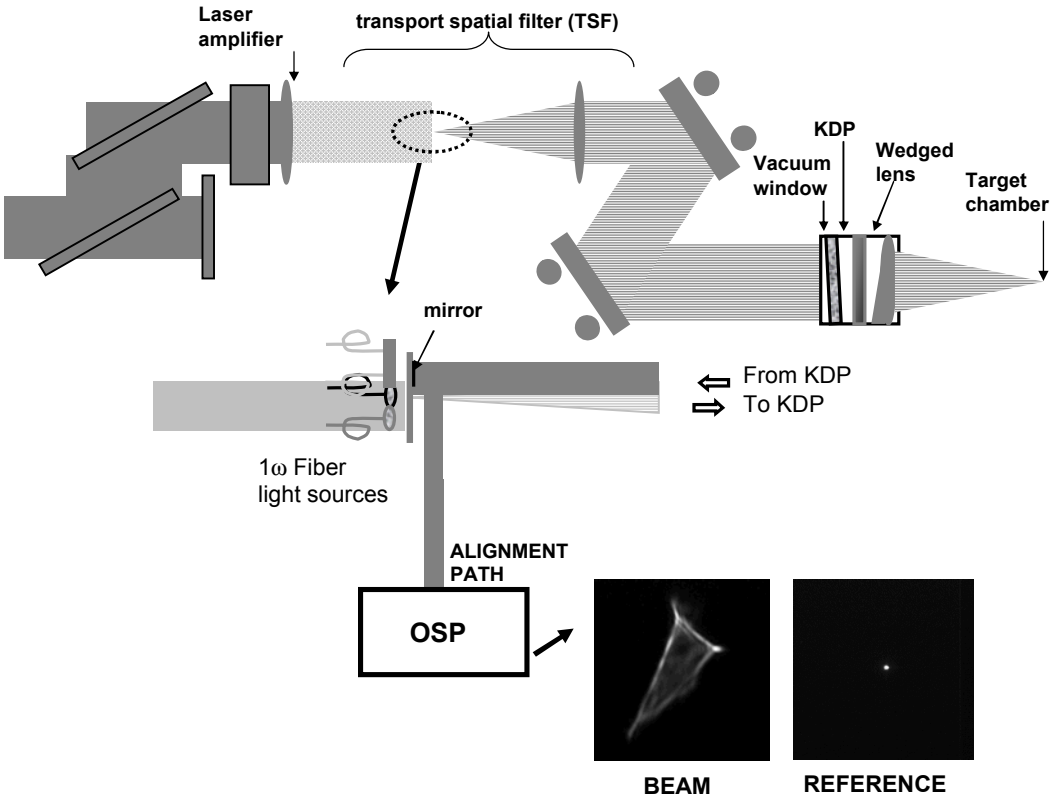

Figure 2. The optical set up for KDP beam alignment.

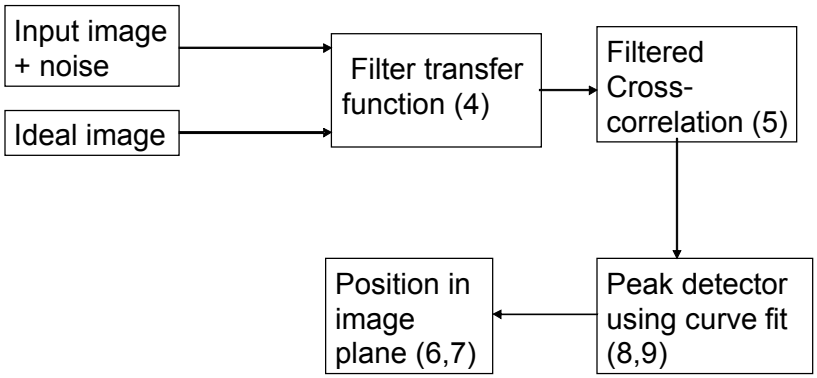

Figure 3. Block diagram of the beam position detection algorithm. Numbers in parenthesis correspond to equation numbers.

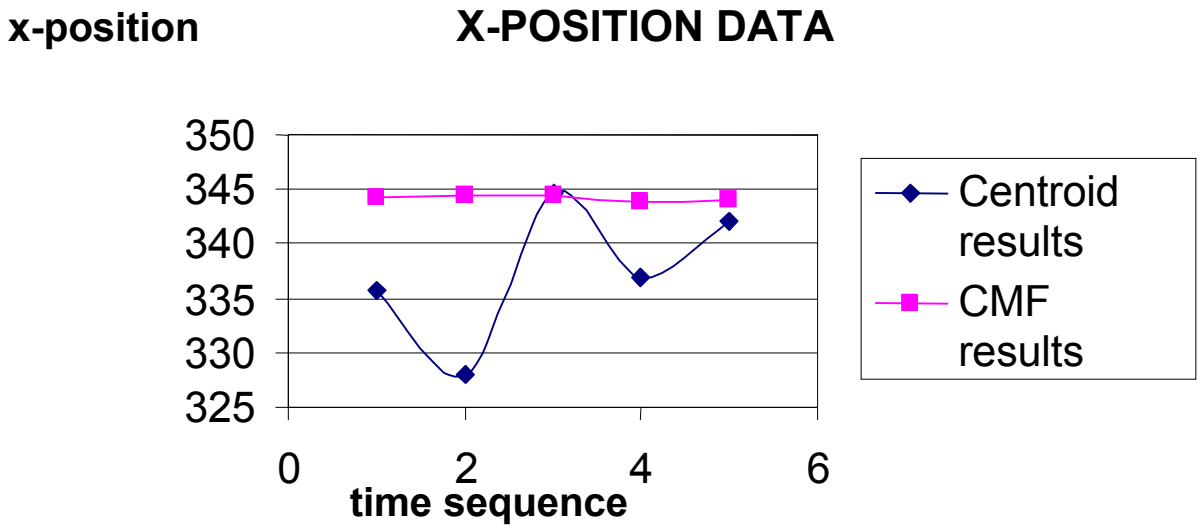

Figure 4. Comparison of the matched filtering method with the binary centroid based method

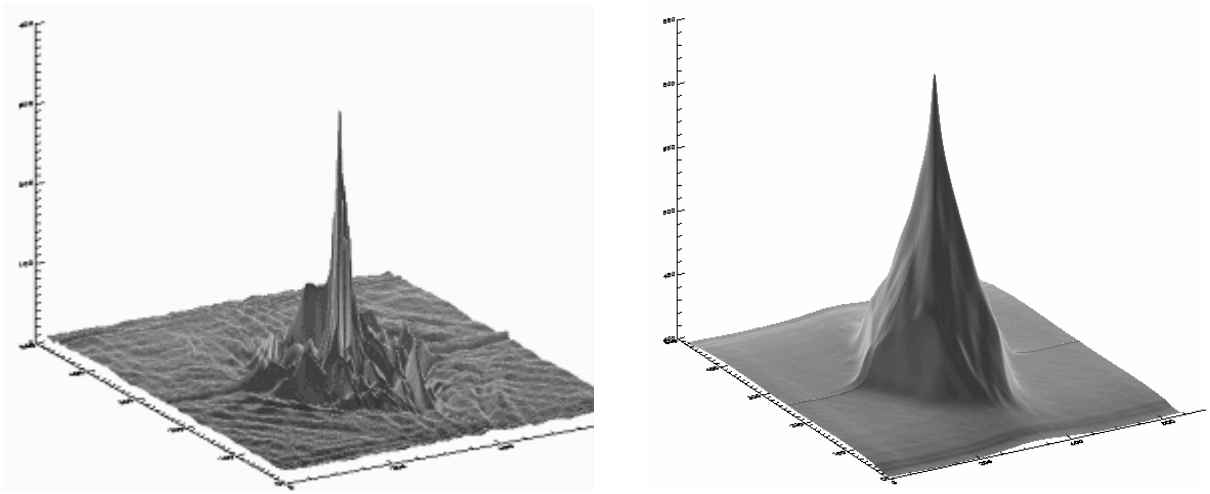

(a) (b)

Figure 5(a). An AMPOF correlation peak (b) A CMF peak has a broad base

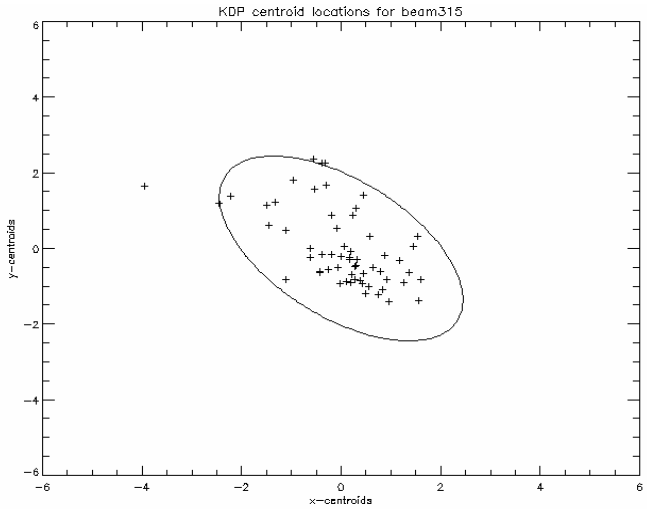

Figure 6. Scatter plot of 49 image positions taken over six months

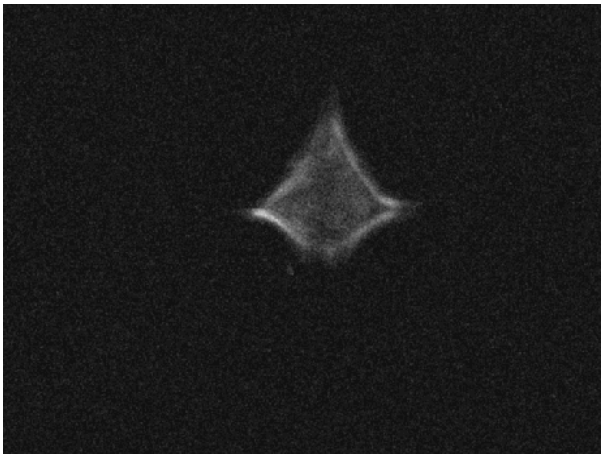

(a)

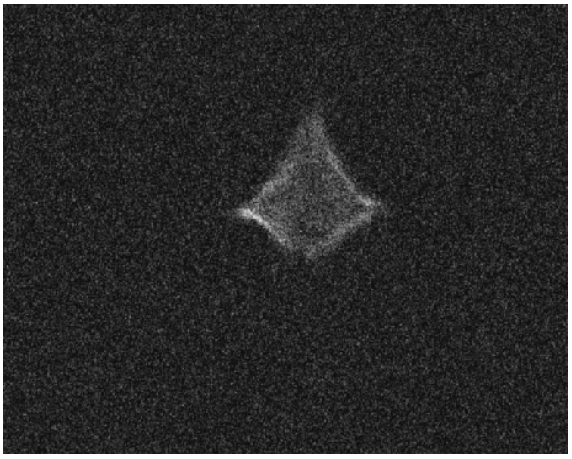

(b)

Figure 7(a). Amplitude max 200, noise 20 rms (b). Amplitude max 200, noise 50 rms

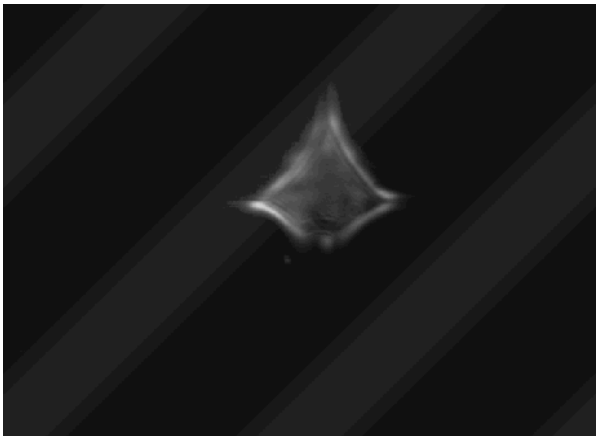

(c)

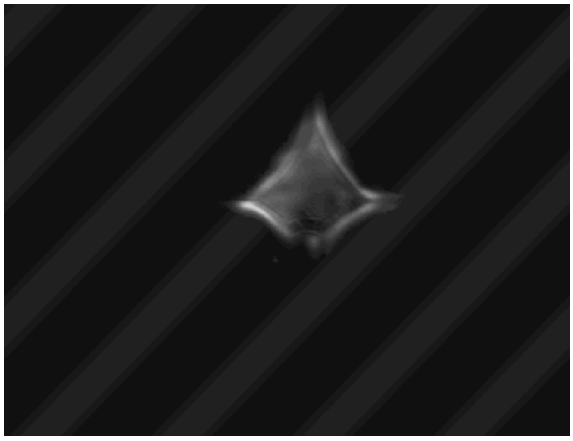

(d)

(c). Amplitude 200, interference 20, period ½λ (d). Amplitude 200, interference 20, period λ

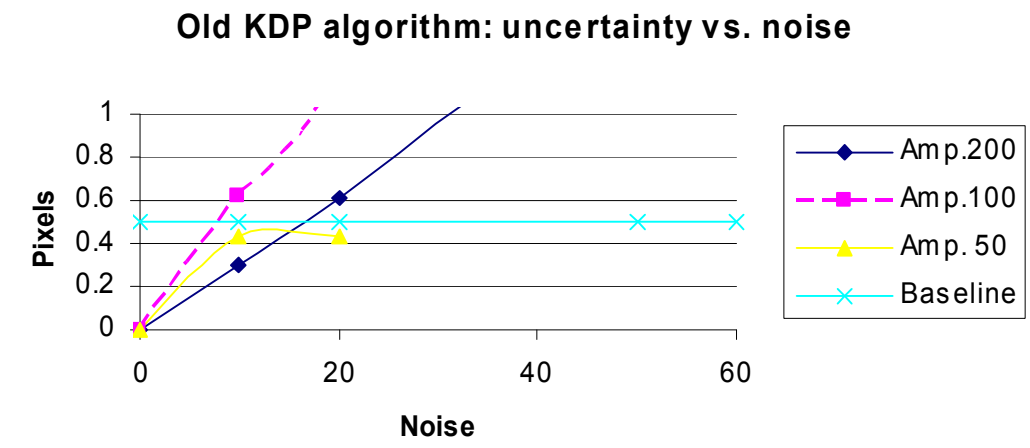

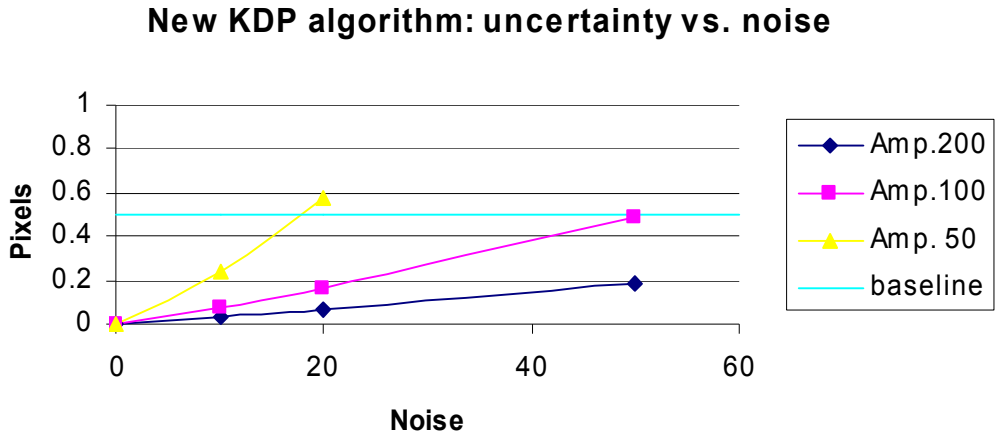

Figure 8(a). Noise versus uncertainty of centroid-based algorithm; noise in rms count and uncertainty in pixels. (b). Noise vs. uncertainty of the AMPOF algorithm.

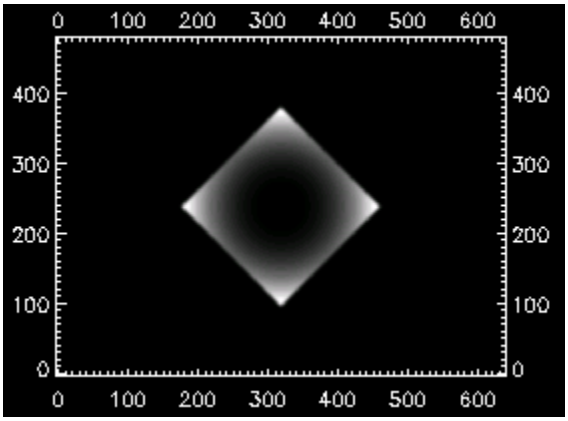

(a)

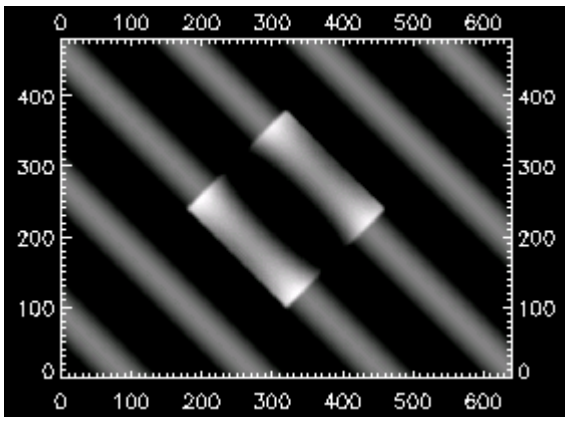

(b)

Figure 9(a) The original image

(b) Amplitude 100, interference amp. 50, 2 wave

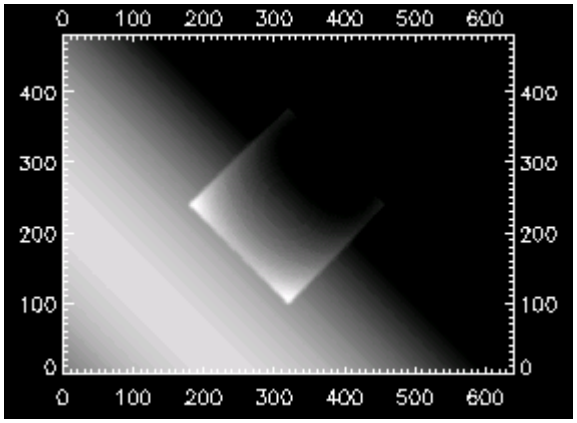

(c)

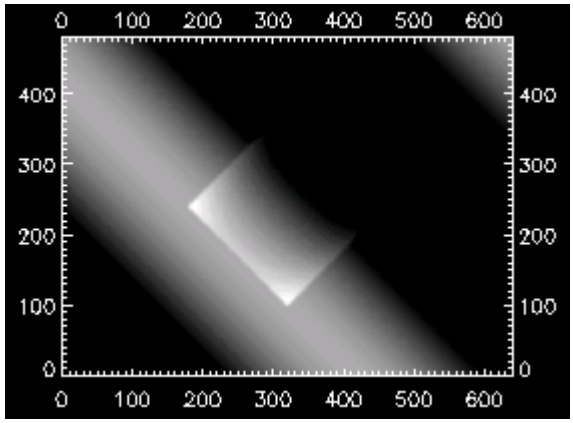

(d)

(c) Amplitude 50, interference amplitude 50, one wave

(d) Amplitude 50, interference amplitude 50, half-wave

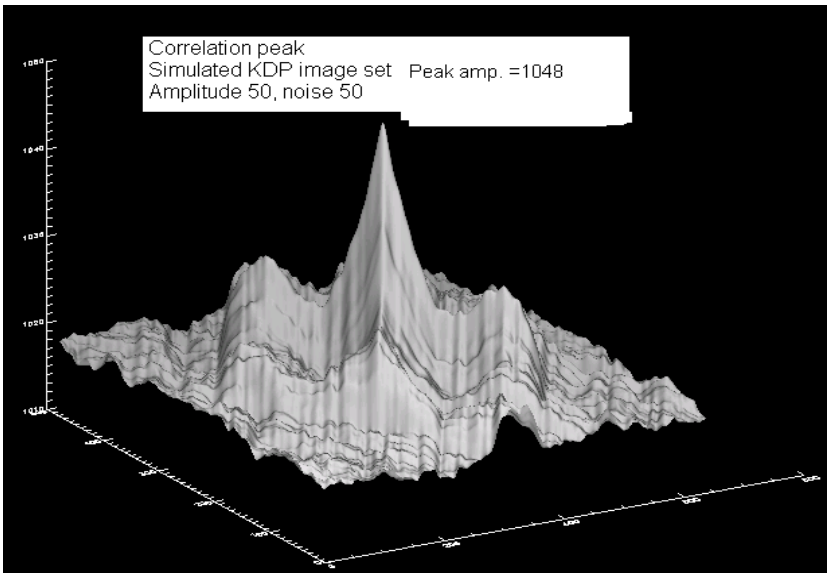

Figure 10. Correlation output for amplitude 50 image corrupted by diffraction amplitude 50, half wave signal

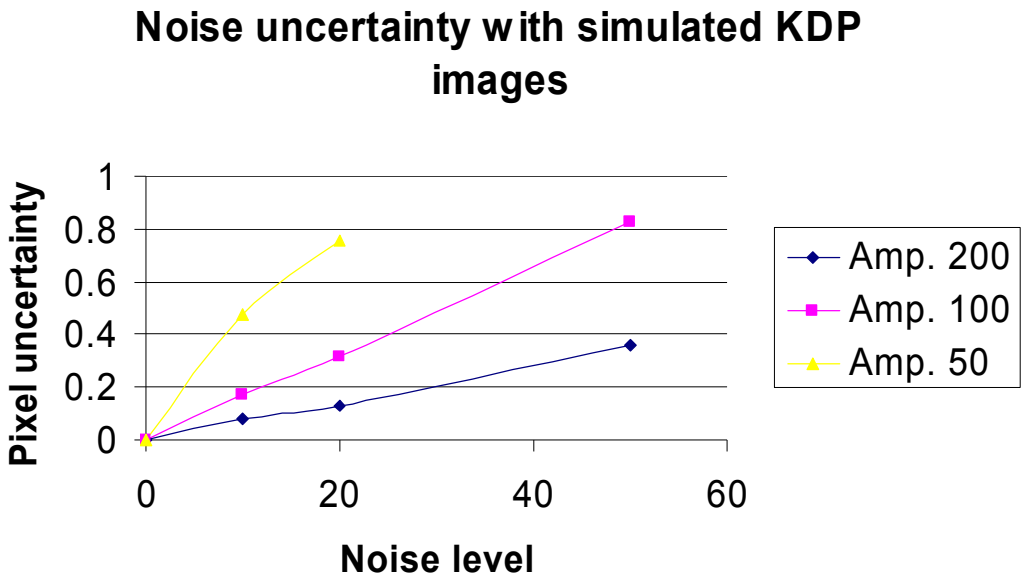

(a)

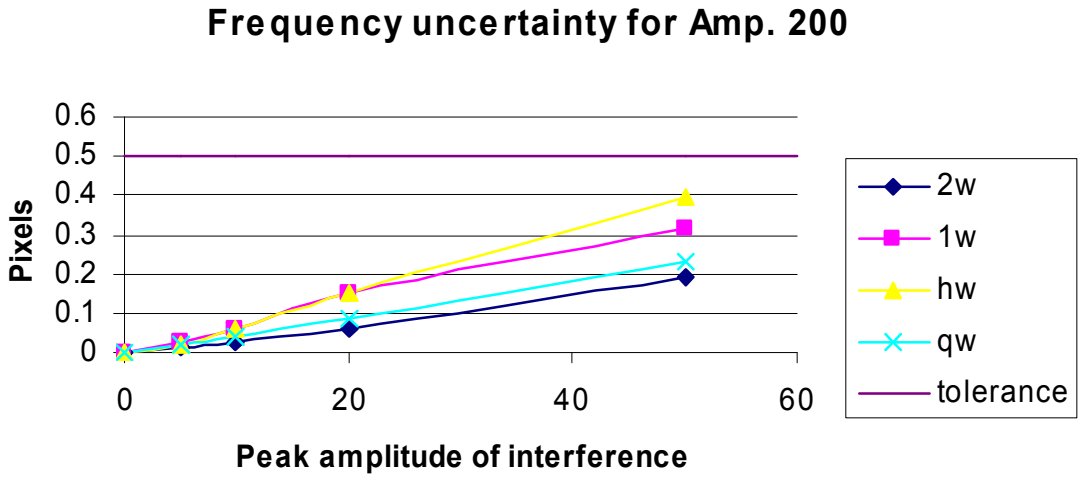

(b)

Figure 11(a). Noise versus uncertainty with AMPOF algorithm amplitude signal and rms noise (b). Noise uncertainty for various wave distortions for various amplitudes of wave

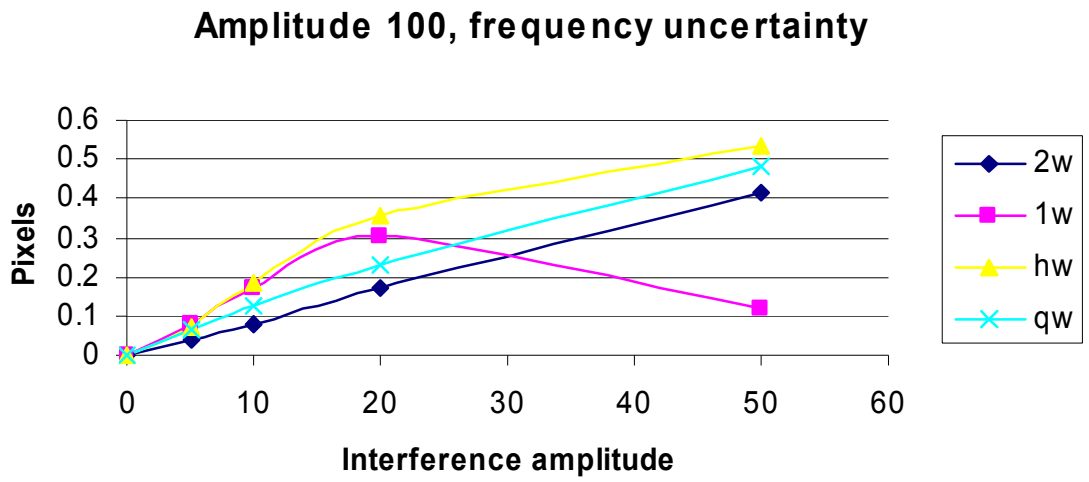

(a)

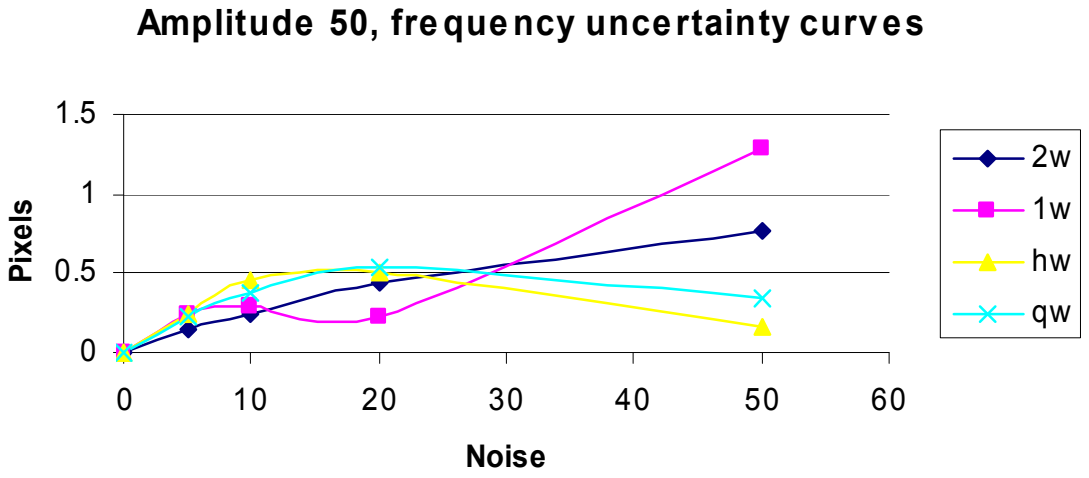

(b)

Figure 12(a). Noise versus uncertainty with new (b). Noise uncertainty for various wave distortions for algorithm for various amplitude signal and rms noise various amplitudes of wave

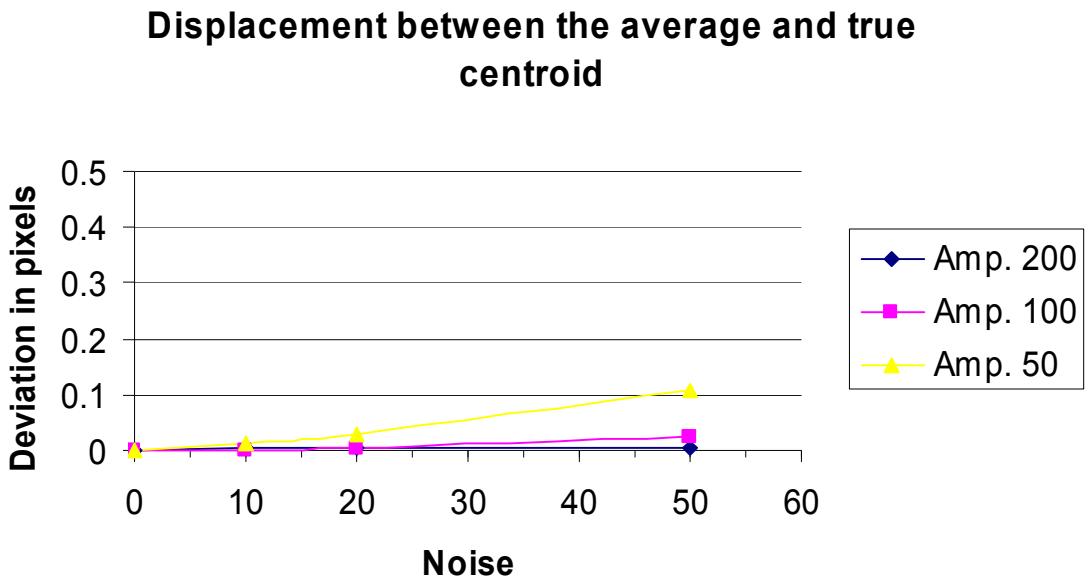

(a)

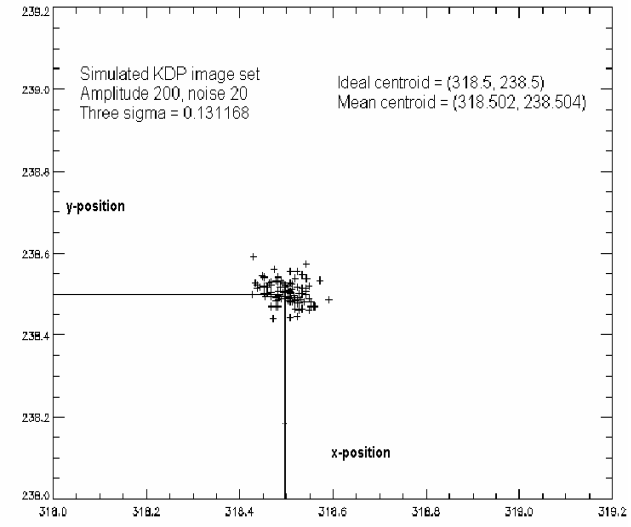

(b)

Figure 13(a). Displacement between the average and true (b). Scatter plot for amplitude 200 with rms noise 20 count centroids for various signal amplitude signal and rms noise

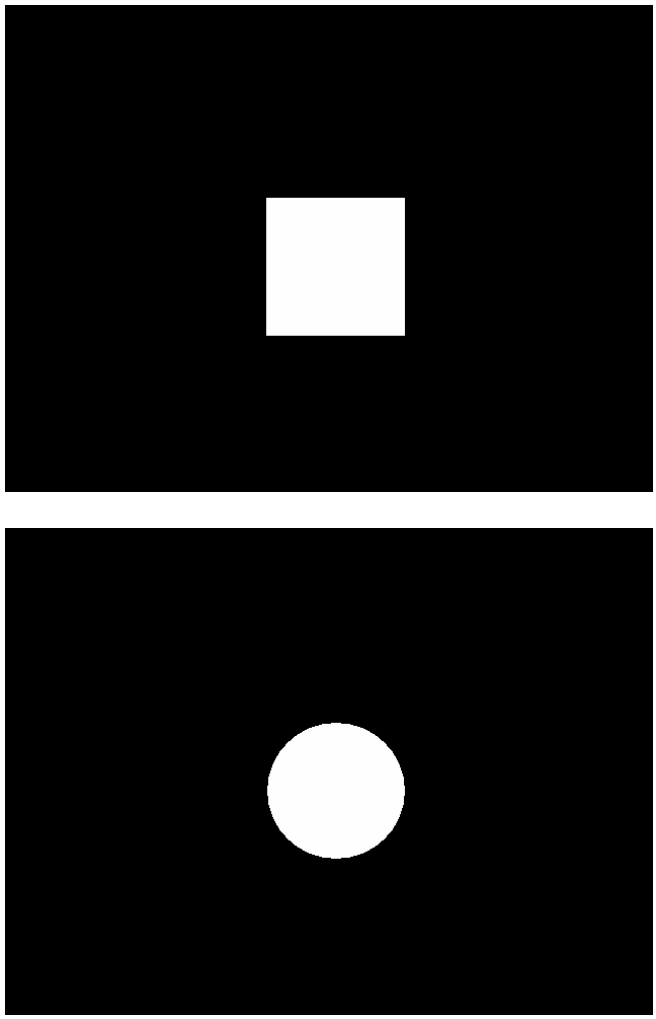

Figure 14. Pedestal experiment performed by correlating the square and the circle shown above. The background is set at 0 and the white region set at 255.

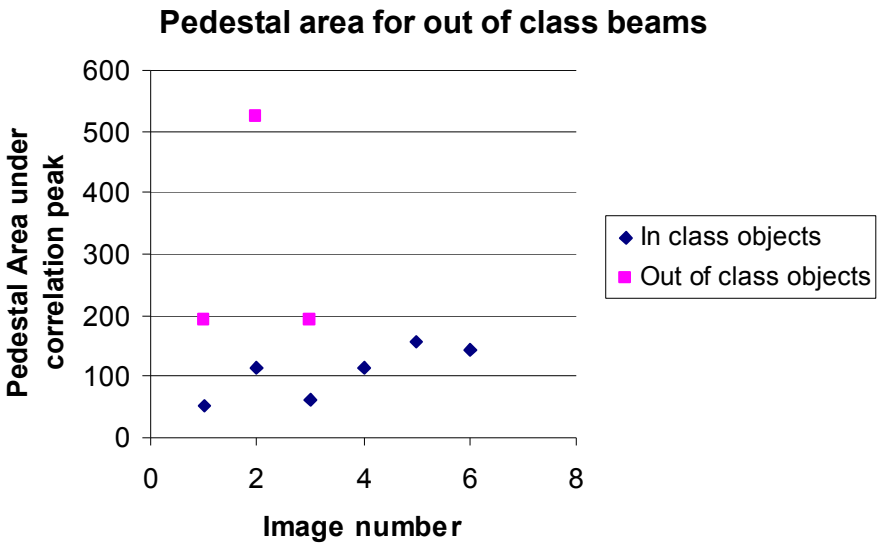

Figure 15. Pedestal area for in-class and out of class beams

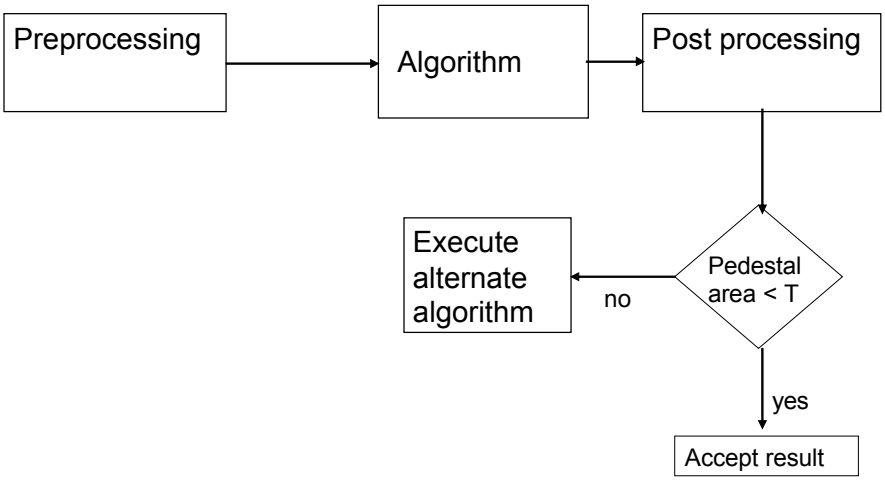

Figure 16. Block diagram of the beam position detection algorithm